

Dark matter halo properties from the power spectrum of density perturbations

Eduard Salvador-Solé¹ and Alberto Manrique¹

¹ Institut de Ciències del Cosmos, Universitat de Barcelona (UB–IEEC),
Martí i Franquès 1, E-08028 Barcelona, Spain.

Abstract

We present a fully analytical derivation of the structural and kinematic properties of dark matter halos in any hierarchical cosmology from the power spectrum of (linear) density perturbations.

1 Introduction

In the last two decades, simulations have provided us with detailed information on the properties of hierarchically assembled virialised cold dark matter (CDM) haloes. However, from the theoretical viewpoint, the situation is far from satisfactory as we do not know how do all these properties come from.

Before the development of simulations, most efforts focused on determining the density profile for objects formed in Secondary Infall (SI), that is in the monolithic collapse of an isolated spherically symmetric seed with outward-decreasing density profile and pure Hubble velocity field [5, 10, 3, 9, 4]. Unfortunately, these models use many approximations (spherical symmetry, radial collapse, the existence of an adiabatic invariant, self-similarity) and unrealistic initial conditions. The question therefore rised about whether or not it was possible to accurately derive the density profile of CDM halos within the SI model.

After the advent of numerical simulations, it become clear that CDM haloes have universal density profiles NFW or Einasto [17, 18, 14, 15]. However, the origin of such a profile is unknown. Is it mainly the effect of smooth accretion or major mergers? How is it at radii below the resolution length of simulations [17, 11, 16]? In addition, simulations show that the kinematic properties of CDM halos are also universal [21, 7, 8]. But how are they set? Recently, it has been shown that all these properties are recovered from SI [23]. But why are they not altered by major mergers?

Here we show how to derive analytically halo properties directly from the power-spectrum of primordial density perturbations. This approach has been presented in [19, 22, 20], hereafter Paper I, II and III, respectively.

2 Halo density profile

We assume SI. However, we do not assume neither spherical symmetry nor radial infall; we adopt the most general point of view that halos are triaxial and collapse through non-radial infall. We do not assume either self-similarity, nor the existence of any adiabatic invariant; we only take into account that halos grow from the inside out as, during virialisation, there is no apocentre-crossing (see Paper I). The inside-out condition then leads to the exact relation (Paper I)

$$r = \frac{3M}{10|E_p(M)|}, \quad (1)$$

telling that the mass profile $M(r)$, readily leading to the spherically averaged density profile $\rho(r)$ of the (triaxial) halo, is determined by the energy

$$E_p(R_p) = 4\pi \int_0^{R_p} dr_p r_p^2 \rho_p(r_p) \left\{ \frac{[H_i r_p - v_p(r_p)]^2}{2} - \frac{GM(r_p)}{r_p} \right\}, \quad (2)$$

associated with identical mass

$$M = 4\pi \int_0^{R_p} dr_p r_p^2 \rho_p(r_p), \quad (3)$$

in the spherically averaged protohalo at any arbitrary small enough cosmic time t_i . In equations (2) and (3), $\rho_p(r_p)$ is the spherically averaged density profile of the protohalo, $H(t_i)$ is the Hubble constant at t_i and $v(r_p)$ is the peculiar velocity at r_p owing to the inner mass excess, to leading order in the deviations from sphericity

$$v_p(r_p) = -\frac{2G \left[M(r_p) - 4\pi r_p^3 \rho_U(t_i)/3 \right]}{3H(t_i)r_p^2}, \quad (4)$$

being $\rho_U(t_i)$ the mean cosmic density.

Protohalos are peaks in the filtered initial density field. Thus, according to the inside-out growth of halos, the region inside any isodensity contour arises from a peak at the corresponding scale. Consequently, the value at $r_p = 0$ of the spherically averaged unconvolved density contrast profile for the seed, $\delta_p(r_p)$, convolved by a Gaussian window of radius R_f is equal to the typical density contrast of typical peaks equally convolved,

$$\delta_{pk}(R_f) = \frac{4\pi}{(2\pi)^{3/2} R_f^3} \int_0^\infty dr_p r_p^2 \delta_p(r_p) e^{-\frac{1}{2} \left(\frac{r_p}{R_f} \right)^2}. \quad (5)$$

$\delta_{pk}(R_f)$ is therefore the Laplace transform of $\delta_p(r_p)$ and, provided it is known, we can invert equation (5) to find $\delta_p(r_p)$ and from it $\rho_p(r_p)$.

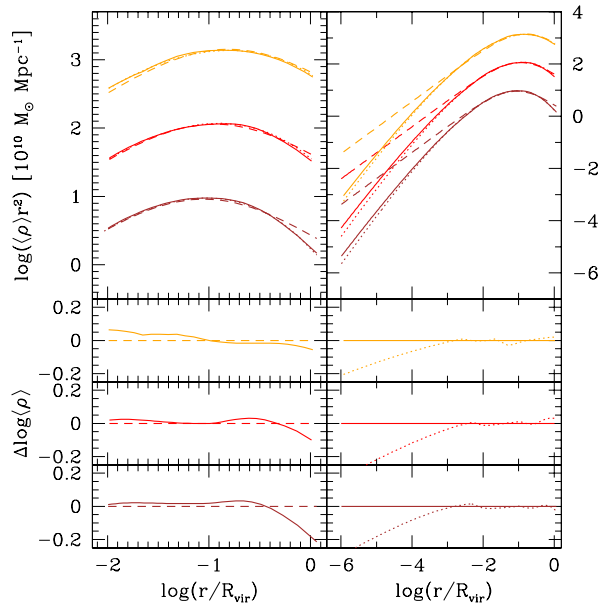


Figure 1: Predicted density profiles (solid lines) for halos with current masses equal to 10, 1 and 0.1 times the critical mass for collapse, $M_* = 3.6 \times 10^{12} M_\odot$ (respectively in orange, red and brown), compared to the density profiles of the NFW (dashed lines) and Einasto (dotted lines) form down to a the typical resolution radius of simulations (left) and four orders of magnitude less (right). To avoid crowding, the curves for $10 M_*$ and $0.1 M_*$ have been respectively shifted upwards and downwards by a factor of 3. The lower panels show the residuals.

In any random Gaussian density fields, $\delta_{pk}(R_f)$ satisfies the differential equation [12, 13]

$$\frac{d\delta_{pk}}{dR_f} = -x_e(R_f, \delta_{pk})\sigma_2(R_f)R_f, \quad (6)$$

where $\sigma_2(R_f)$ is the second order spectral moment and $x_e(R_f, \delta_{pk})$ is the average curvature x of typical peaks with δ_{pk} at R_f (see [12, 13] for its form as a function of the spectral moments). Equation (6) can be solved for the boundary condition leading to the wanted halo with mass M at t . We can then calculate $E_p(M)$ (eqs. [2] and [3]) and, from equation (1), obtain the wanted halo density profile $\rho(r)$. In Fig. 1, we compare the density so derived with the MFW and Einasto profile for CDM halos of the masses. The agreement is excellent.

But why do mergers not modify this profile? From equation (1), we see that given any arbitrary virialised halo, we can always think about one protohalo evolving into it through SI. And we can assume this origin because virialisation is a true relaxation, so the memory of the true initial conditions has been lost.

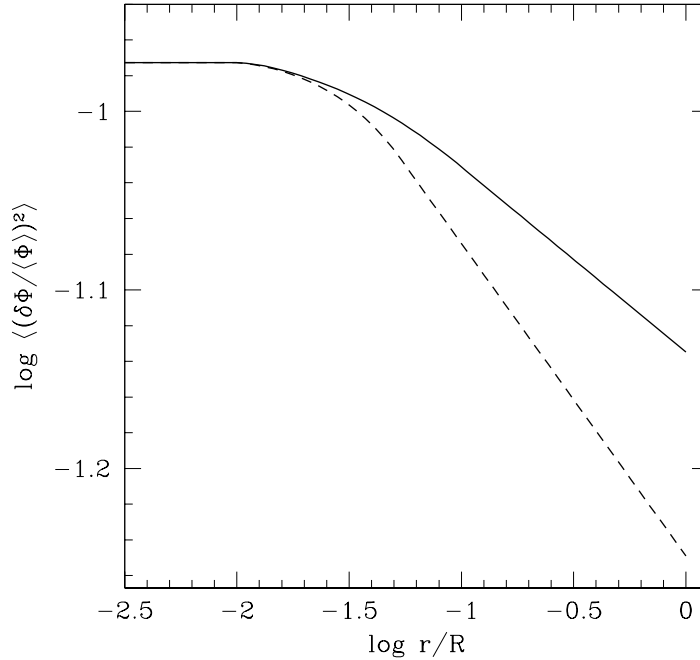


Figure 2: Typical mean squared potential fluctuation profiles according to the typical eccentricity of peaks (solid line) and a small variation of it (dashed line).

3 Halo kinematics and triaxial shape

The kinematic and triaxial shape of halos can also be derived. To this end, we must adopt the same conditions as above for the density profile plus the following extra assumption: in non-radial infall part of the radial kinetic energy of particles is transferred to the tangential kinematic energy without altering their total energy.

Indeed, the inside-out growth allows one to relate eccentricity profiles to the protohalo squared semi-axis ratio profiles (see Paper III for details), through three Laplace transforms. The eccentricity of typical peaks in the primordial density field filtered at different scales is well known [2]. Thus, we can once again invert those relations and find the eccentricity profile of CDM halos resulting from peaks by SI.

From the eccentricity profiles, we can readily derive the rms dimensionless potential fluctuation profile, $\langle (\delta\Phi / \langle \Phi \rangle)^2 \rangle^{1/2}$. Then, the extra assumption above allows us to write

$$\frac{\sigma_t^2(r)}{\sigma^2(r)} = \left\langle \left(\frac{\delta\Phi}{\langle \Phi \rangle} \right)^2 \right\rangle^{1/2} (r), \quad (7)$$

allowing one to determine the anisotropy profile. And, making use of the Jeans equation for anisotropic triaxial systems in equilibrium (see Paper II), the velocity dispersion profile.

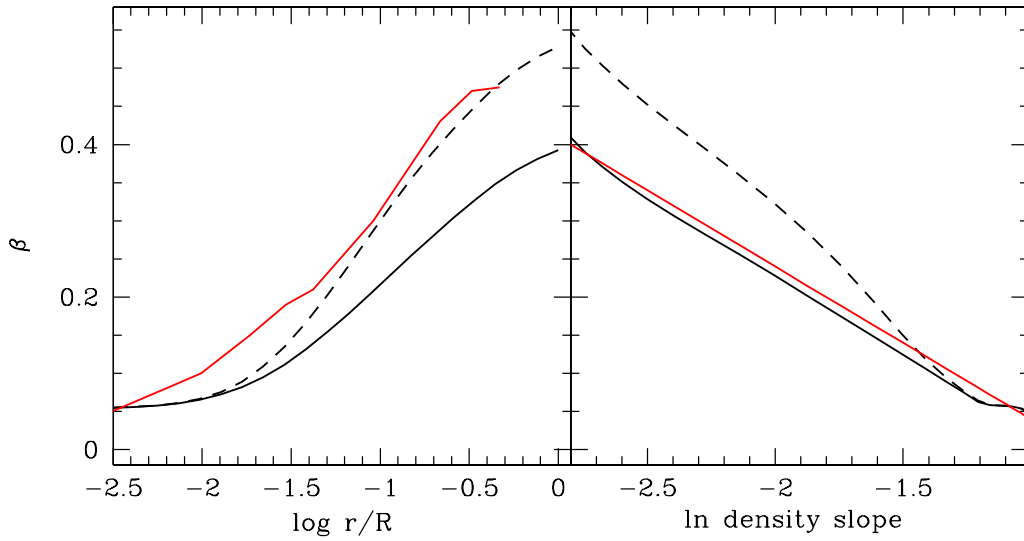


Figure 3: Anisotropy profile derived from the rms potential fluctuation profiles shown in Fig. 2 (same lines), as a function of radius (left) for the comparison with the curve found by [18] for a simulated Milky Way halo (red line) and as a function of the logarithmic density slope for comparison with the expression by [8].

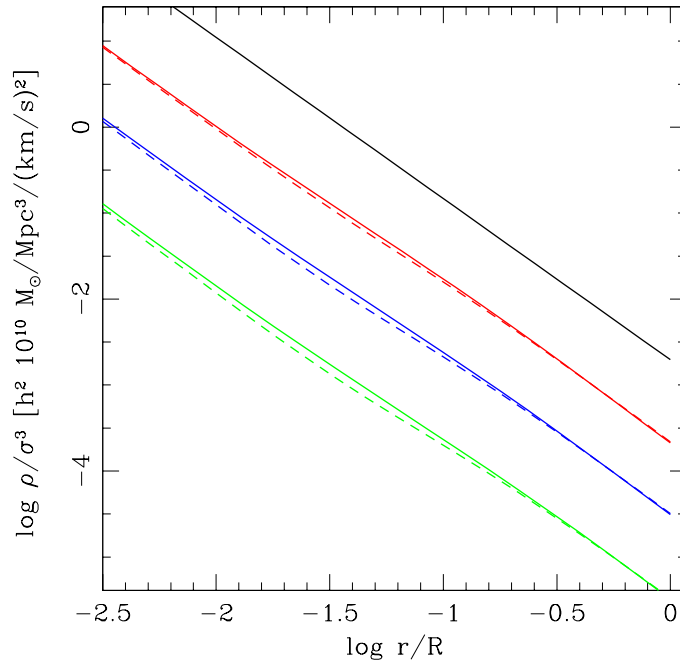


Figure 4: Corresponding pseudo phase-space density profiles (same lines). The straight line in black (with arbitrary zero-point) is the typical profile found in simulations. We also plot the results for haloes with $10^{13} M_\odot$ (blue lines) and $10^{14} M_\odot$ (green lines).

In Fig. 2, we plot the rms potential fluctuation profile predicted from the typical eccentricities of peaks and a small variation of it. The halo anisotropy and velocity dispersion (actually the pseudo-phase space density $\rho(r)/\sigma^3(r)$) profiles arising from them are given in Figs. 3 and 4. These kinematic profiles are in full agreement with the results obtained in numerical simulations. On the other hand the halo eccentricity profiles are also consistent with those predicted by this theory.

Acknowledgments

This work was supported by the Spanish DGES, AYA2009-12792-C03-01, and the Catalan DIUE, 2009SGR00217.

References

- [1] Ascasibar, Y., Yepes, G., Gottlöber, S., & Müller, V. 2004, MNRAS, 352, 1109
- [2] Bardeen, J. M., Bond, J. R., Kaiser, N., & Szalay, A. S. 1986, ApJ, 304, 15
- [3] Bertschinger, E. 1985, ApJS, 58, 39
- [4] Del Popolo, A., Gambera, M., Recami, E., & Spedicato E. 2000, A&A, 353, 427
- [5] Gunn, J. E. 1977, ApJ, 218, 592
- [6] Gunn, J. E. & Gott, J. R. 1972, ApJ, 176, 1
- [7] Hansen, S. H., & Moore, B. 2006, New Astronomy, 11, 333
- [8] Hansen, S. H. & Stadel, J. 2006, JCAP, 5, 14
- [9] Hoffman, Y. & Shaham, J. 1985, ApJ, 297, 16
- [10] Fillmore, J. A. & Goldreich, P. 1984, ApJ, 281, 1
- [11] Fukushige, T. & Makino, J. 1997, ApJ, 477, L9
- [12] Manrique, A. & Salvador-Solé, E. 1995, ApJ, 453, 6
- [13] Manrique, A. & Salvador-Solé, E. 1996, ApJ, 467, 504
- [14] Merritt, D., Navarro, J. F., Ludlow, A., & Jenkins, A. 2005, ApJ, 624, L85
- [15] Merritt, D., Graham, A. W., Moore, B., Diemand, J., & Terzić, B. 2006, AJ, 132, 2685
- [16] Moore, B., Governato, F., Quinn, T., Stadel, J., & Lake, G. 1998, ApJ, 499, L5
- [17] Navarro, J. F., Frenk, C. S., & White, S. D. M. 1997, ApJ, 490, 493
- [18] Navarro, J. F., Hayashi, E., Power, C., et al. 2004, MNRAS, 349, 1039
- [19] Salvador-Solé, E., Viñas, J., Manrique, A., & Serra, S. 2012, MNRAS, 423, 2190
- [20] Salvador-Solé, E., Serra, S., Manrique, A., & González-Casado, G. 2012, MNRAS, 424, 3129
- [21] Taylor, J. E., & Navarro, J. F. 2001, ApJ, 563, 483
- [22] Viñas, J., Salvador-Solé, E., & Manrique, A. 2012, MNRAS, 424, L6
- [23] Wang, J. & White, S. D. M. 2009, MNRAS, 396, 709